

Characterizing Quantum-Dot Cellular Automata

Burkhard Ritter
Supervised by Prof. Dr. Kevin Beach

May 2014

Contents

1	Approximations	5
---	----------------	---

Chapter 1

Approximations

To access larger systems we need to introduce approximations. Approximating means to simplify. However, by carefully establishing successive approximations and their limits, we also reduce the problem to its essential ingredients and thus, hopefully, we gain a better understanding of the system. Our first approximation is somewhat ad hoc and motivated by the very ideas underlying the QCA approach. QCA relies on two electrons per cell (or, more generally, a fixed number of charges per cell). Therefore we truncate the Hilbert space and keep only states with two electrons in each cell. We omit the chemical potential term, $\mu = 0$. This *fixed charge* approximation obviously does not allow for charge fluctuations and consequently cannot accommodate inter-cell hopping. We justify the approximation by noting that, at least in principle, for any given cell layout we can always tune the system parameters (especially the chemical potential) so that we have two electrons per cell. Of course, in practice there are very clear limits as to how much system parameters can be tuned and any QCA cell layout considered within the *fixed charge* approximation cannot necessarily be readily implemented on a given real-world material system.

For the *fixed charge* system, the state space scales as $N_s = \binom{8}{2}^{N_c} = 28^{N_c}$ (N_c is the number of cells). Again, we utilize symmetries to make the Hamiltonian matrix block diagonal and as before the largest block is the spin zero sector, of size $N'_s = 16^{N_c}$. This corresponds to a memory consumption of 512kB, 128MB, and 32GB for two, three and four cell systems, respectively. That's doable. Five cells, however, remain impossible. To illustrate how the approximation works Fig. ??(a) compares the density of states (more correctly, the energy state histogram) of both the *fixed charge* and the exact *grand canonical* system. The *fixed charge* approximation accurately reproduces the low-energy spectrum of the *grand canonical* model. This is not unexpected. As long as the QCA system is in the right regime, the two-electrons-per-cell sector is lowest in energy. It is in this limit, with the temperature additionally smaller than the energy gap to the next higher charge sector, that the approximation is valid. Fig. ??(b) demonstrates the breakdown of the approximation. Here we have plotted the particle number per cell over temperature and as

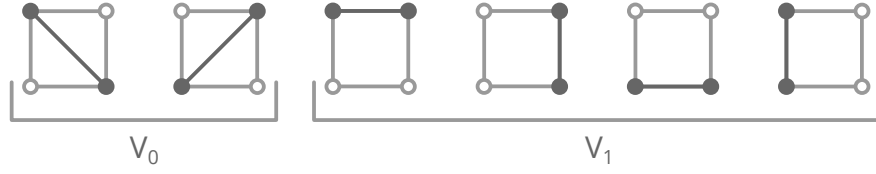


Figure 1.1: ...

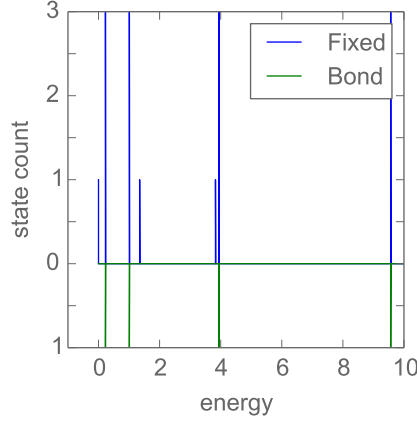


Figure 1.2: Low-energy density of states of a one cell QCA system for both the *fixed charge* and the *bond* model. The *bond* approximation does not reproduce the singlet-triplet splitting.

the temperature is increased and becomes comparable to the energy gap, the *fixed charge* and *grand canonical* systems diverge.

As evidenced by our semi-classical introduction at the beginning of this report, the QCA approach does not consider particle spins. It solely relies on charge-charge interactions. Therefore it is natural to the QCA approach to neglect the spin degree of freedom as a next step. The 28 states per cell of the *fixed charge* model can be reorganized into four doubly occupied dots and six bonds, four along the edges and two along the diagonals of the cell. Each bond consists of two electrons and corresponds to four states, one spin singlet and three spin triplets. By keeping only one state for each bond and omitting the doubly occupied states we arrive at the *bond* approximation. It has a basis of six states per cell, the six bonds. As a consequence, the size of the Hilbert space is $N_s = 6^{N_c}$ (N_c the number of cells). Five and six cells are doable, with memory requirements of 460MB and 16GB, respectively, whereas seven cells are not (580GB). Note that for the *bond* model there are no symmetries that can be exploited.

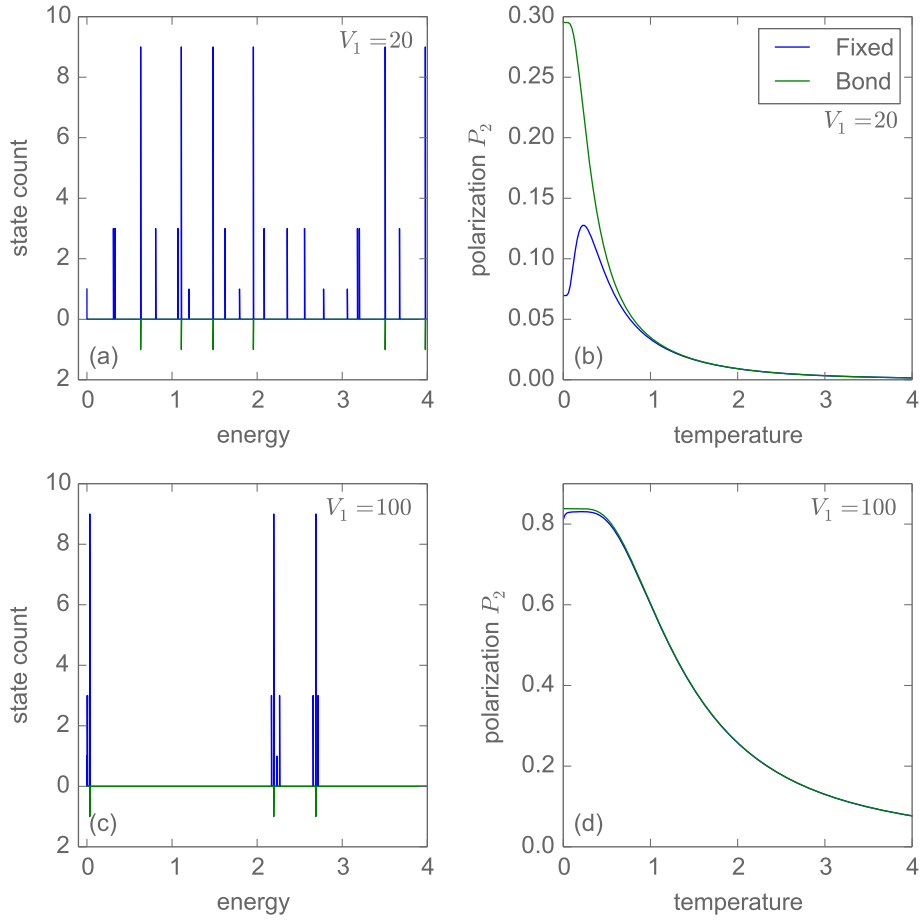


Figure 1.3: The two cell *fixed charge* and *bond* systems at $V_1 = 20$ and $V_1 = 100$. (a)(c) Low-energy density of states. (b)(d) Output polarization P_2 over temperature. For a small Coulomb repulsion the density of states curves look qualitatively very different (a) and the *bond* approximation does not work very well (b). At a larger Coulomb repulsion the density of states curves look much more alike (c) and the *bond* approximation works much better (d).

Apart from requiring sufficiently gapped out doubly occupied states, the *bond* approximation assumes that the bond singlet and triplet states are energetically degenerate. But this is not quite correct. To understand how the approximation works we look at the density of states (energy state histogram, to be correct) of the single cell *fixed charge* and *bond* systems, Fig. 1.2. Each *bond* state maps to three *fixed charge* states—the triplet—and one “close-by” state—the singlet. Hence, singlet and triplet states are not equivalent, they are split by an energy gap ΔE . We speculate that, similar to the antiferromagnetic Heisenberg coupling constant J emerging in the low energy limit of the Hubbard model (with $J \sim \frac{t^2}{U}$) [1], here, virtual excitations to high energy doubly occupied states lower the energy of the singlet state compared to the triplet state. Since the *bond* model ignores the singlet-triplet splitting it is important to understand how this gap depends on various system parameters. To that end we picked out a few selected singlet-triplet states from the spectrum in Fig. 1.2 as examples. Contrary to expectations, for those states the gap ΔE did not change significantly with the on-site Coulomb repulsion U , however, it did decrease with decreasing b , the inter-cell spacing. Most importantly, for the nearest-neighbour Coulomb potential, $V_1 = \frac{1}{a}$ (a being the cell side length), we found $\Delta E \sim \frac{1}{V_1^p}$. The exponent is $p \sim 3$ when the cell “sees” a biasing external potential (e.g. $P_0 = \pm 1$) and $p \sim 1$ otherwise (e.g. $P_0 = 0$). Even though our method is anything but rigorous and the obtained results very likely not universally true, the findings should nonetheless give a good enough idea of the principle trends. Quite generally, the higher the overall Coulomb potential (large V_1 , small b), the smaller the singlet-triplet splitting and, conceivably, the more accurate the *bond* approximation.

We expect the approximation to work as long as the singlet-triplet splitting is “washed out,” that is, as long as the temperature is much bigger than the gap ΔE . As a very, very rough estimate we come up with $T \gg \frac{t^2}{V_1}$. Of course, we also need $T \ll U$ so that the doubly occupied states are gapped out. Outside of this loosely defined regime, the *bond* model can and does go terribly wrong. Especially the ground state is often qualitatively completely incorrect. Consider, for example, Fig. 1.3(b) where we have plotted the output polarization P_2 of a two cell system over temperature. For this system we set the input polarization $P_0 = 1$, the Hubbard U is practically infinite, the inter-cell spacing is $b = 2a$, and the nearest-neighbour Coulomb repulsion has the value $V_1 = \frac{1}{a} = 20$ (in units of t , $t = 1$). The two curves for the *fixed charge* and the *bond* system disagree at low temperatures. It is instructive to compare the density of states of the two systems, Fig. 1.3(a): They look quite different, qualitatively. In that light it is rather remarkable that the polarization curves actually agree quite well at higher temperatures ($T > 1$). The *bond* model only reproduces the most populous energy states of the exact spectrum. Apparently, that is enough to give (almost) correct results at high temperatures. The lower the temperature, the more important become the few lowest lying energy states which the *bond* model misses. For a larger Coulomb repulsion, $V_1 = 100$, the density of states curves look much more alike, even though the *bond* model obviously still does not resolve all the lines of the exact

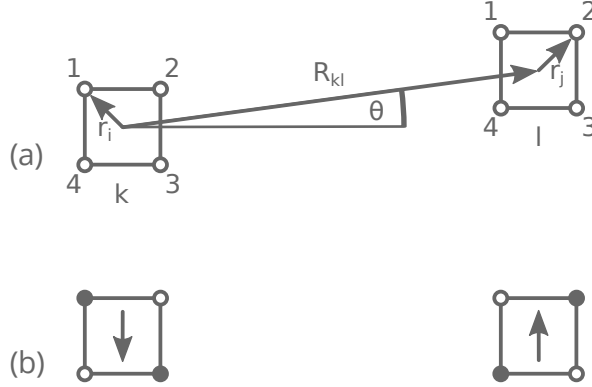


Figure 1.4: a) QCA cells k and l . b) The two-states-per-cell approximation identifies each cell with a spin \uparrow or \downarrow .

spectrum, Fig. 1.3(c). Accordingly, the approximation works much better as can be seen in Fig. 1.3(d). As a last remark, note that for the two cell system each single *bond* state corresponds to 16 ($4 \cdot 4$) *fixed charge* states.

A linear array of QCA cells where each cell has a state of digital 0 or 1 is reminiscent of a 1D spin $\frac{1}{2}$ chain. Indeed, if we reduce the basis to only two states per cell (down from six states in the *bond* picture) we can map the QCA system to a transverse-field Ising model. This is an attractive proposition: The smaller Hilbert space allows for larger system sizes with our exact diagonalization method; much more importantly, the transverse-field Ising model is amenable to sign-problem-free Stochastic series expansion (SSE) quantum Monte Carlo schemes [?]. These methods do not scale exponentially¹ and consequently allow access to much larger systems. Last, but not least, such a mapping connects the QCA approach to the established and well studied Ising model. The prospect hinges on the assumption that the two-states-per-cell basis actually is a good approximation for QCA systems. And while two-state cells are certainly the picture we have in mind when we talk about QCA it is not a priori clear whether this is a correct physical picture. We have yet to investigate the validity of the approximation. However, an Ising model with long-ranged interactions, *inspired* by QCA, is an interesting and worthwhile problem in its own right.

To map the two-states-per-cell QCA system to an Ising model, we first identify each cell k with a spin σ_k^z . More precisely, digital 0 corresponds to \downarrow and digital 1 to \uparrow , see Fig. 1.4(b). The Hamiltonian can now be rewritten as a sum over single cell kinetic terms

¹SSE quantum Monte Carlo methods roughly scale as $N \ln N$ where N is the system size.

H_k and Coulombic cell-cell interactions terms V_{kl} ,

$$\begin{aligned} H &= - \sum_{\langle ij \rangle \sigma} t c_{i\sigma}^\dagger c_{j\sigma} + \sum_{i < j} V_{ij} n_i n_j \\ &= \sum_k \hat{H}_k + \sum_{k < l} V_{kl} . \end{aligned} \quad (1.1)$$

We expect the single cell H_k to map to a transverse field term $-\gamma \sigma_k^x$. However, here we focus on the cell-cell interaction term exclusively. Its full expression is

$$V_{kl} = \sum_{ij} \frac{n_i n_j}{|\mathbf{R}_{kl} + \mathbf{r}_j - \mathbf{r}_i|} , \quad (1.2)$$

where i and j sum over the four dots $1 \dots 4$ of cell k and l , respectively; \mathbf{R}_{kl} denotes the vector between the centres of the cells, see Fig. 1.4(a). There are only four possibilities for two interacting cells: $\uparrow\uparrow$, $\downarrow\downarrow$, $\uparrow\downarrow$, and $\downarrow\uparrow$. Using a multipole expansion and keeping terms up to $\mathcal{O}\left(\frac{a^4}{R^5}\right)$, the four corresponding energies $V_{kl}^{\uparrow\uparrow}$, $V_{kl}^{\downarrow\downarrow}$, $V_{kl}^{\uparrow\downarrow}$, and $V_{kl}^{\downarrow\uparrow}$ can be calculated separately. Due to the inherent geometrical symmetries of the problem and due to the fact that the dipole moment vanishes for the two cell states \uparrow and \downarrow , the obtained expressions are not too unwieldy. It turns out that $V_{kl}^{\uparrow\downarrow} = V_{kl}^{\downarrow\uparrow}$. Hence we have a three-level system which we cannot hope to represent by a solely two-level Ising term $J_{kl} \sigma_k^z \sigma_l^z$. Instead we try to map to a cell-cell Hamiltonian of the form

$$H_{kl} = J_{kl} \sigma_k^z \sigma_l^z + J'_{kl} (\sigma_k^z + \sigma_l^z) . \quad (1.3)$$

For this Hamiltonian we have the energies (omitting the indices k and l for brevity)

$$E^{\uparrow\uparrow} - E^{\uparrow\downarrow} = 2J + 2J' \quad (1.4)$$

$$E^{\downarrow\downarrow} - E^{\uparrow\downarrow} = 2J - 2J' \quad (1.5)$$

which yields

$$J = \frac{1}{4} (E^{\uparrow\uparrow} + E^{\downarrow\downarrow} - 2E^{\uparrow\downarrow}) \quad (1.6)$$

$$J' = \frac{1}{4} (E^{\uparrow\uparrow} - E^{\downarrow\downarrow}) . \quad (1.7)$$

By identifying $E^{\uparrow\uparrow} = V_{kl}^{\uparrow\uparrow}$, $E^{\downarrow\downarrow} = V_{kl}^{\downarrow\downarrow}$, and so on, we obtain the final expressions

$$J = \frac{1}{32} \frac{9a^4 - 105a^4 \cos 4\theta}{R^5} \quad (1.8)$$

$$J' = -\frac{1}{4} \left(\frac{6a^2 \sin 2\theta}{R^3} + \frac{5a^4 \sin 2\theta}{R^5} \right) . \quad (1.9)$$

In the limit $\frac{a}{R} \ll 1$ and together with the (conjectured) kinetic single cell term $-\gamma\sigma_k^x$ we have thus mapped the two-state QCA system to a transverse-field Ising model, albeit with an additional J' term. The interactions decrease as $\frac{1}{R^3}$ and $\frac{1}{R^5}$ for J' and J , respectively. Both J and J' vary with the angle θ between the two cells. As a consequence, different directions prefer different cell configurations ($\uparrow\uparrow$ versus $\downarrow\downarrow$) and only few select angles yield a pure Ising interaction $J_{kl}\sigma_k^z\sigma_l^z$ —for example a linear array of cells ($\theta = 0^\circ$). This is significant as it breaks the symmetry between digital 0 and 1 (spin \downarrow and \uparrow) for QCA devices if we are not very careful in how we engineer them. Moreover, the pure Ising interaction seems to be quite fragile with respect to angle displacement, as demonstrated in Fig. ??.

Here we have plotted the energies $E^{\uparrow\uparrow} = J + 2J'$, $E^{\downarrow\downarrow} = J - 2J'$, and $E^{\uparrow\downarrow} = E^{\downarrow\uparrow} = -J$.

Bibliography

- [1] A. Auerbach, *Interacting electrons and quantum magnetism*. Graduate texts in contemporary physics. Springer New York, 1994.
<http://books.google.ca/books?id=tiQlKzJa6GEC>.